

# Author's Accepted Manuscript

Structural Chemistry and Magnetic Properties of  
 $LnMnFeGe_4O_{12}$  ( $Ln = Y, Eu, Lu$ )

Diming Xu, Maxim Avdeev, Peter D. Battle, J.M.  
Cadogan, Henry Lamont



PII: S0022-4596(17)30253-0  
DOI: <http://dx.doi.org/10.1016/j.jssc.2017.06.032>  
Reference: YJSSC19850

To appear in: *Journal of Solid State Chemistry*

Received date: 31 May 2017

Revised date: 27 June 2017

Accepted date: 30 June 2017

Cite this article as: Diming Xu, Maxim Avdeev, Peter D. Battle, J.M. Cadogan and Henry Lamont, Structural Chemistry and Magnetic Properties of  $LnMnFeGe_4O_{12}$  ( $Ln = Y, Eu, Lu$ ), *Journal of Solid State Chemistry* <http://dx.doi.org/10.1016/j.jssc.2017.06.032>

This is a PDF file of an unedited manuscript that has been accepted for publication. As a service to our customers we are providing this early version of the manuscript. The manuscript will undergo copyediting, typesetting, and review of the resulting galley proof before it is published in its final citable form. Please note that during the production process errors may be discovered which could affect the content, and all legal disclaimers that apply to the journal pertain.

# Structural Chemistry and Magnetic Properties of $LnMnFeGe_4O_{12}$ ( $Ln = Y, Eu, Lu$ )

Diming Xu<sup>1</sup>, Maxim Avdeev<sup>2,3</sup>, Peter D. Battle<sup>1,\*</sup>, J. M. Cadogan<sup>4</sup>,  
Henry Lamont<sup>1</sup>

<sup>1</sup>Inorganic Chemistry Laboratory, Oxford University, South Parks Road, Oxford OX1 3QR,  
U.K.

<sup>2</sup>Australian Nuclear Science and Technology Organisation, Lucas Heights, NSW2234,  
Australia

<sup>3</sup>School of Chemistry, The University of Sydney, Sydney, NSW2006, Australia

<sup>4</sup>School of Physical, Environmental and Mathematical Sciences, UNSW Canberra at the  
Australian Defence Force Academy, Canberra BC 2610, Australia

\*Corresponding author: peter.battle@chem.ox.ac.uk

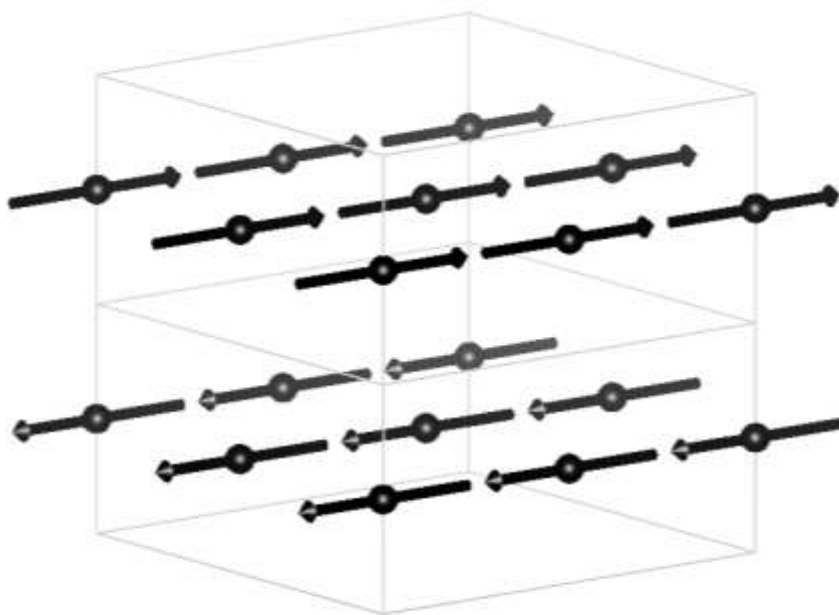
## Abstract

Polycrystalline samples of  $LnMnFeGe_4O_{12}$  ( $Ln = Y, Eu, Lu$ ) have been prepared using the ceramic method and characterised by a combination of magnetometry, Mössbauer spectroscopy, X-ray diffraction and neutron diffraction. They all adopt the space group  $P4/nbm$  with  $a \sim 9.670$ ,  $c \sim 4.81$  Å and show long-range antiferromagnetic order with transition temperatures  $15 \leq T_N/K \leq 17$ . The magnetic structure is the same in each case and consists of an A-type ordering of (001) planes; the ordered spins lie in the (001) plane. Comparison with isostructural compounds leads to the conclusion that subtle structural

changes play a greater role than the electronic configuration of the cation in determining the magnetic structure.

# Graphical abstract

$LnMnFeGe_4O_{12}$  ( $Ln = Y, Eu, Lu$ ) order as A-type antiferromagnets with  $15 \leq T_N/K \leq 17$



Keywords: A-type antiferromagnet; neutron diffraction

## Introduction

Over the years, magnetic superexchange interactions that involve multi-atom pathways, sometimes dubbed super-superexchange interactions, have been the focus of many studies, both experimental and computational, with arsenates, phosphates, sulfates and germanates being amongst the compounds investigated [1-4]. Our own recent research has centred on the family of germanates described by the general formula  $AM_{2-x}M'_x\text{Ge}_4\text{O}_{12}$ , where  $M$  and  $M'$  are paramagnetic cations and  $A$  is a diamagnetic cation. We are attempting to elucidate the factors that influence the strength of the magnetic superexchange interactions through tetrahedral  $[\text{GeO}_4]^{4-}$  groups and, concomitantly, the consequences for the magnetic properties of replacing a magnetically isotropic cation, for example  $\text{Mn}^{2+}$ , with an anisotropic cation, for example  $\text{Co}^{2+}$ , over a wide composition range,  $0 \leq x \leq 2$ . To date, we have reported on  $\text{CeMn}_{2-x}\text{Co}_x\text{Ge}_4\text{O}_{12}$  [5] and  $\text{ZrMn}_{2-x}\text{Co}_x\text{Ge}_4\text{O}_{12}$  [6]. The tetragonal crystal structure adopted by these systems is illustrated in Figure 1; the unit cell parameters are  $a \sim 9.8 \text{ \AA}$ ,  $c \sim 4.9 \text{ \AA}$ , that is  $c \sim a/2$ . The  $2b$  site of space group  $P4/nbm$  is occupied by the tetravalent cation and the  $4f$  site by a disordered distribution of divalent cobalt and manganese. These two cation sites are coordinated by eight and six oxygen atoms, respectively, and have square-antiprismatic and octahedral geometries. They can be considered to lie in layers perpendicular to the  $[001]$  axis. These layers are separated from each other by layers containing  $[\text{Ge}_4\text{O}_{12}]^{8-}$  rings, each ring being comprised of four vertex-sharing  $\text{GeO}_4$  tetrahedra. The  $d$ -block cations form a pseudo-cubic structure with a unit-cell parameter of  $a/2$  ( $\sim c$ ) and the magnetic ordering patterns that they adopt at low temperatures can thus be described using the notation introduced by Wollan and Koehler [7]. Both  $\text{CeMn}_2\text{Ge}_4\text{O}_{12}$  and  $\text{ZrMn}_2\text{Ge}_4\text{O}_{12}$  adopt the C-type antiferromagnetic structure drawn [8] in Figure 2(a), with the ordered magnetic moments aligned along  $[001]$ . In each case the replacement of 25 % of the  $\text{Mn}^{2+}$  cations by  $\text{Co}^{2+}$  results in a rotation of the moments into the  $(001)$  plane, see Figure 2(b), and, although the underlying C-type structure is retained, there is evidence for a small degree of spin canting. The magnetic structure of the zirconium-based system does not then undergo any major change as the  $\text{Co}^{2+}$  concentration is increased through the range  $0.25 \leq x \leq 2.0$ , although the weak ferromagnetism caused by the spin canting grows in strength. In contrast, the cobalt-rich compositions  $\text{CeMn}_{0.5}\text{Co}_{1.5}\text{Ge}_4\text{O}_{12}$  and  $\text{CeCo}_2\text{Ge}_4\text{O}_{12}$  adopt a non-collinear, antiferromagnetic structure with a unit cell that is doubled along  $[001]$ , see Figure 2(c). This magnetic structure can be considered to have G-type ordering along  $[100]$  and a weaker A-type component along  $[010]$ . Furthermore, the application of a 20 kOe magnetic field results in a halving of the volume of the magnetic unit

cell and the adoption of a weakly-ferromagnetic C-type structure, see Figure 2(b). We do not presently have a satisfactory explanation for the difference in behaviour of the zirconium- and cerium-based systems. The difference in the ionic radii of the two tetravalent cations will lead to subtle structural differences. It will also lead to a difference in their acidities, that is the extent to which they compete with the *d*-block cations for the anion electron density that plays a crucial role in the superexchange interactions. More data are needed if we are to establish which factors are most important in determining the magnetic structures adopted by these compounds. To this end we have now conducted a study of the mixed manganese/iron compositions  $LnMn_{2-x}Fe_xGe_4O_{12}$  for  $Ln = Y, Eu$  and  $Lu$ . The results of our investigations are described below.

## Experimental

Attempts were made to prepare polycrystalline samples of  $LnMn_{2-x}Fe_xGe_4O_{12}$  for  $Ln = Y, Eu$  and  $Lu$  and  $0 \leq x \leq 2$  using the ceramic method. Stoichiometric quantities of  $MnCO_3$ ,  $Fe_3O_4$  and dried  $Ln_2O_3$  were mixed and ground together with a 5 % excess of  $GeO_2$ . After an initial heating in powder form at 1075 °C the reaction mixture was pelletised and heated, again at 1075 °C, for several days. The mixture was reground and repelleted at least every 48 h. The reaction was deemed to be complete when the X-ray powder-diffraction (XRPD) pattern of the product did not change between successive firings. The XRPD pattern of the final product was recorded at room temperature using a Panalytical X'pert diffractometer operating with monochromated Cu  $K\alpha_1$  radiation. Data were collected in the range  $10 \leq 2\theta/^\circ \leq 130$  with a step size  $\Delta 2\theta = 0.0084^\circ$  and analysed by the Rietveld method [9] as implemented in the GSAS [10] program suite. The magnetic properties of the reaction products were measured with a Quantum Design MPMS 5000 SQUID magnetometer. For each sample the dc magnetic susceptibility was measured in an applied field of 100 Oe over the temperature range  $2 \leq T/K \leq 300$  after both zero-field-cooling (ZFC) and field-cooling (FC) and the field dependence of the magnetization was measured at 2 K over the field range  $-50 \leq H/kOe \leq 50$ . In the case of  $LuMnFeGe_4O_{12}$  the ac susceptibility was measured as a function of frequency over the temperature range  $2 \leq T/K \leq 30$ . Neutron powder-diffraction (NPD) data were collected at room temperature and 3.5 K on the high-resolution powder diffractometer Echidna at ANSTO. The angular range of  $8 \leq 2\theta/^\circ \leq 160$  was scanned using a step size of  $\Delta 2\theta = 0.05^\circ$  with a wavelength of 1.622 Å or 2.4397 Å. The sample was loaded in powder

form into a cylindrical vanadium can that was mounted in a closed-cycle refrigerator. In the case of  $Ln = \text{Eu}$ , the sample was mounted in an annular space within the cylinder in an attempt to minimise absorption effects. Rietveld analysis of the data was carried out using the peak shape function developed by van Laar and Yelon [11]. An absorption correction was applied in the case of  $Ln = \text{Eu}$ . The correction factor, calculated on the basis of the sample mass and geometry, was held constant during the data analysis.

An  $^{57}\text{Fe}$  Mössbauer spectrum was collected from a polycrystalline sample of  $\text{YMnFeGe}_4\text{O}_{12}$  at 295 K using a standard transmission spectrometer and a  $^{57}\text{CoRh}$  source. The drive velocity of the spectrometer was calibrated using a 6  $\mu\text{m}$  thick  $\alpha\text{-Fe}$  foil, at 295 K, and the isomer shift ( $\delta$ ) is quoted relative to the centre of the  $\alpha\text{-Fe}$  calibration spectrum. The spectrum was fitted using the NORMOS software [12].

## Results

XRPD showed that our attempts to prepare  $Ln\text{Mn}_{2-x}\text{Fe}_x\text{Ge}_4\text{O}_{12}$  for  $Ln = \text{Y}$ ,  $\text{Eu}$  and  $\text{Lu}$  across the whole composition range  $0 \leq x \leq 2$  were unsuccessful. In this paper we shall focus on the composition  $Ln\text{MnFeGe}_4\text{O}_{12}$  which could be prepared as a single phase using each of the lanthanide elements under consideration. The X-ray diffraction pattern in each case could be indexed in the tetragonal space group  $P4/nbm$  with the iron and manganese cations disordered over the  $4f$  site; the fitted X-ray diffraction pattern of the sample  $Ln = \text{Y}$  is shown in Figure 3. The corresponding diagrams for  $Ln = \text{Eu}$ ,  $\text{Lu}$  are shown in Figures S1 and S2. The neutron diffraction patterns recorded at room temperature were also consistent with this space group. They are shown, along with the calculated patterns, in Figures 4, S3 and S4 for  $Ln = \text{Y}$ ,  $\text{Eu}$  and  $\text{Lu}$ , respectively. There was no evidence for the symmetry lowering that would be necessary in order to accommodate an ordered arrangement of the  $d$ -block cations. The structural parameters derived from the NPD data are listed in Table 1 and the corresponding bond lengths and bond angles are given in Table 2. The square antiprism around the  $2b$  site is formed by eight equidistant O2 anions. The Mn/Fe atom on the  $4f$  site is coordinated by two *trans* O1 ions and four O2 ions; these will subsequently be referred to as the axial and planar sites of the octahedron, respectively. Each germanium atom is coordinated by two O1 and two O2 atoms at the vertices of a tetrahedron.

The room-temperature Mössbauer spectrum of  $\text{YMnFeGe}_4\text{O}_{12}$  is shown in Figure 5 and the parameters used to fit it are listed in Table 3.

The temperature dependence of the molar magnetic susceptibility of the three  $LnMn_{2-x}Fe_xGe_4O_{12}$  compositions is shown in Figure 6 and the field dependence of the magnetisation in Figure 7. The parameters derived by fitting the data in the temperature range  $150 \leq T/K \leq 300$  to the Curie-Weiss law are listed in Table 4. The ac susceptibility of  $LuMnFeGe_4O_{12}$  is shown in Figure 8.

Neutron diffraction data were collected on each sample at 3.5 K using wavelengths of both 1.622 and 2.4397 Å. In all cases, Bragg peaks that were not present at 300 K were observed at low scattering angles, suggesting that a transition to a magnetically-ordered state had occurred on cooling. There was no evidence to suggest that the structural space group  $P4/nbm$  had not been retained. The observed and calculated low-temperature diffraction patterns for  $Ln = Y$  are shown in Figure 9; those for  $Ln = Eu$  and  $Lu$  are shown in Figures S5 and S6. In each case, the magnetic structure drawn in Figure 10 was used to model the magnetic scattering. The antiferromagnetic structure, described by the magnetic space group  $P2_1c/b'an$  (#50.9.385), consists of an A-type ordering of (001) planes with the atomic moments aligned along [100]. The magnitudes of the ordered cation moments refined to be 4.06(2), 4.37(8) and 3.75(2)  $\mu_B$  for  $Ln = Y$ ,  $Eu$  and  $Lu$ , respectively. The atomic parameters derived from the data collected using a wavelength of 1.622 Å are listed in Table S1 and the corresponding bond lengths and bond angles are given in Table S2.

## Discussion

In contrast to the previously reported systems  $CeMn_{2-x}Co_xGe_4O_{12}$  and  $ZrMn_{2-x}Co_xGe_4O_{12}$ , there is some ambiguity concerning the cation oxidation states in  $LnMnFeGe_4O_{12}$ . The transition-metal cations could exist either as  $Mn^{3+}$  and  $Fe^{2+}$  or as  $Mn^{2+}$  and  $Fe^{3+}$ . The pseudo-tetragonal coordination geometry around the  $4f$  site might be expected to favour the formation of  $Mn^{3+}$  with a  $3d^4$  electron configuration whereas the lower third ionisation energy of iron will favour the formation of  $Fe^{3+}$ . Our study of  $YMnFeGe_4O_{12}$  by Mössbauer spectroscopy was intended to resolve this issue but the data are somewhat inconclusive. The isomer shift, see Table 3, is consistent with the presence of high-spin, spherical  $Fe^{3+}$  cations but the quadrupole splitting is unusually large for such a species. The alternative explanation, based on the presence of aspherical  $Fe^{2+}$ , is more consistent with the magnitude of the quadrupole splitting but the observed isomer shift is significantly lower than would be expected in that case. The observation of an effective magnetic moment of  $\sim 5.9 \mu_B$  for all  $Ln$  strongly suggests that all the cations have  $3d^5$  electron configurations and that  $Mn^{2+}$  and  $Fe^{3+}$

cations are therefore present. In that case, the quadrupole splitting of 2.086(2) mm s<sup>-1</sup> is unusually large for a high-spin Fe<sup>3+</sup> compound [13]. The cause of the splitting is discussed below. We should also point out that although Eu<sup>3+</sup> has a non-magnetic ground state, a partially-occupied excited state with  $J \neq 0$  often contributes to the measured susceptibility and the observation of a Curie constant as low as 8.758(1) cm<sup>3</sup> K mol<sup>-1</sup> might be considered surprising. However, as we emphasise below, the coordination geometry around the Eu<sup>3+</sup> cations in EuMnFeGe<sub>4</sub>O<sub>12</sub> is unusually compressed, and this is likely to have consequences for the magnetic properties.

The two, very different, Mn/Fe – O bond lengths around the 4*f* sites in *Ln*MnFeGe<sub>4</sub>O<sub>12</sub> create a pseudo-tetragonal environment for the *d*-block cation, although the true site symmetry is monoclinic, 2/*m*. The electric-field gradient created by the irregular coordination sphere is presumably responsible for the large quadrupole splitting observed in the Mössbauer spectrum. The mean Mn – O and Fe – O bond lengths in MnO and Fe<sub>2</sub>O<sub>3</sub> are 2.222 and 2.029 Å, respectively, and a mean bond length of ~ 2.126 Å might therefore be expected around the 4*f* site. The observed values are only slightly longer than this, see Table 2. The mean *Ln* – O bond lengths around the 8-coordinate *Ln* cations in *Ln*FeO<sub>3</sub> are 2.428, 2.479 and 2.396 Å for *Ln* = Y, Eu, and Lu, respectively [14-16]. These are all significantly longer than the distances listed in Table 2 for *Ln*MnFeGe<sub>4</sub>O<sub>12</sub>. The bond-valence sums around *Ln* in the germanates are calculated to be 3.46, 3.53 and 3.28, again suggesting that these cations are in relatively compressed environments; the degree of “over-bonding” increases with the ionic radius of *Ln*<sup>3+</sup>. This is consistent with the failure of ourselves and others [17] to prepare isostructural germanates containing *Ln*<sup>3+</sup> cations larger than Eu<sup>3+</sup>. The near-constancy of the Ge – O and mean Mn/Fe – O bond lengths, see Table 2, might lead to a description of the structure as a framework of fixed-size octahedra and tetrahedra with *Ln*<sup>3+</sup> cations occupying a set of 8-coordinate holes. This would be an over-simplification that fails to take into account the structural changes that accompany the variation in size of *Ln*<sup>3+</sup>. The way in which the structure accommodates these changes can be deduced from Table 5 and Figure S7, which include data from our previous studies of CeMn<sub>2-x</sub>Co<sub>x</sub>Ge<sub>4</sub>O<sub>12</sub> and ZrMn<sub>2-x</sub>Co<sub>x</sub>Ge<sub>4</sub>O<sub>12</sub>. The *d*-block cations in CeMn<sub>2</sub>Ge<sub>4</sub>O<sub>12</sub> and ZrMn<sub>2</sub>Ge<sub>4</sub>O<sub>12</sub> are isoelectronic with those in *Ln*MnFeGe<sub>4</sub>O<sub>12</sub> and they can therefore be included in a comparison without introducing variations that should be attributed to changes in orbital occupancy. The data tabulated for these five compositions show that a reduction in the relative size of the cations on the 4*f* and 2*b* sites causes a systematic decrease in the angle,  $\psi$ , between the long axis of the Mn/FeO<sub>6</sub> octahedra and the (001) plane and an increase in the angle,  $\phi$ , between the long and short axes



of the octahedra. The ratio of the bond lengths  $d(\text{Mn/Fe} - \text{O2})/d(\text{Mn/Fe} - \text{O1})$  shows a general decrease with decreasing  $\langle r_{4f} \rangle / r_{2b}$  but it appears to reach a limiting value as the size of the  $\text{Ln}^{3+}$  cation increases and the structure approaches the limit of its stability range. With the exception of the link between  $\varphi$  and the ratio  $\langle r_{4f} \rangle / r_{2b}$ , these observations are robust when the non-isoelectronic compositions detailed in Table 5 are included in the comparison. We therefore conclude that in order to accommodate variations in the size of the  $4f$  cation the pseudo-tetragonal strain within the octahedra is modified and they rotate relative to (001). Table 5 also details the concomitant variation in shape of the square-antiprismatic arrangement of anions around the  $2b$  site using the parameter  $q$ , the ratio of the O2 – O2 distance within a square face to the perpendicular distance between the two such faces.

The temperature dependence of the molar magnetic susceptibility above 150 K is well-modelled by the Curie-Weiss law, see Figure 6. Although the Weiss temperature,  $\theta$ , decreases with the ionic radius of  $\text{Ln}$ , each of the three compositions shows evidence of a transition at  $\sim 16$  K, see Table 4. In the case of  $\text{Ln} = \text{Y}$  or  $\text{Eu}$  the transition is signalled by a maximum in both the ZFC and FC susceptibilities, whereas for  $\text{Ln} = \text{Lu}$  the susceptibility shows a negative gradient across the whole of the measured range. No hysteresis between the ZFC and FC data is observed and the field dependence of the magnetisation is also reversible, see Figure 7. The data thus suggest that  $\text{YMnFeGe}_4\text{O}_{12}$  and  $\text{EuMnFeGe}_4\text{O}_{12}$  adopt antiferromagnetic ground states. The absence of hysteresis in the behaviour of  $\text{LuMnFeGe}_4\text{O}_{12}$  and the absence of any frequency dependence in the ac susceptibility, see Figure 8, rule out the formation of a weakly ferromagnetic state or a spin glass. The magnetometry data suggest that this composition might be an antiferromagnet in which a small fraction of the spins remain paramagnetic below the Néel temperature. This residual paramagnetism could be attributable to the disordered distribution of cations on the  $4f$  site and the disruption of the O – Ge – O superexchange pathways that would be expected to accompany it. However, it is not clear why this disorder only manifests itself in this way when  $\text{Ln} = \text{Lu}$ . The cause could lie in the small structural differences that develop as the radius of  $\text{Ln}^{3+}$  decreases, or it might lie in the relatively-high acidity of the smaller cation and its consequent ability to compete for the electron density in the superexchange pathway. The relatively low value of the ordered cation moment determined by neutron diffraction for  $\text{LuMnFeGe}_4\text{O}_{12}$  is consistent with this explanation. The values measured for the  $\text{Y}^{3+}$  - and  $\text{Eu}^{3+}$  - containing compositions lie within the range observed previously in comparable compounds [2, 3]. Magnetic structures similar to that adopted by the three  $\text{LnMnFeGe}_4\text{O}_{12}$  compositions have previously been observed in  $\text{CeMn}_{0.5}\text{Co}_{1.5}\text{Ge}_4\text{O}_{12}$  and  $\text{CeCo}_2\text{Ge}_4\text{O}_{12}$ . They were described by the same magnetic space

group but in those cases the structure had both a G-type component and an A-type component and, unlike in  $LnMnFeGe_4O_{12}$ , there was evidence of a high-field metamagnetic transition in  $M(H)$ . The changes in magnetic structure observed previously across the series  $CeMn_{2-x}Co_xGe_4O_{12}$  lead us to suggest that the occurrence of a doubled magnetic unit cell and the location of the ordered moment within the (001) plane might both be attributable to the presence of the single-ion anisotropy associated with  $Co^{2+}$  but the magnetic structures determined in the current study show that this is not the case. They are closer to that of  $CeCo_2Ge_4O_{12}$  than to that of  $CeMn_2Ge_4O_{12}$ , a compound that also contains only spherical, high-spin  $d^5$  transition-metal cations. Consideration of the structural data in Table 5 allows us to identify structural factors that correlate with the unit-cell doubling. It seems that this is most likely to occur when the cation radius ratio  $\langle r_{4f} \rangle / r_{2b}$  is small and therefore the ratio of the bond lengths  $(Mn/Fe - O_2)/(Mn/Fe - O_1)$  and the angle between the  $Mn/Fe - O_1$  bond and the (001) plane are small. It is likely that these structural parameters strongly influence the relative strengths of the different superexchange interactions that operate within the structure [5] and hence control the magnetic structure.

## Conclusion

The compounds  $LnMnFeGe_4O_{12}$  ( $Ln = Y, Eu, Lu$ ) are essentially isostructural and they all adopt the same antiferromagnetic structure below  $\sim 16$  K, although there is evidence of residual paramagnetism below  $T_N$  when  $Ln = Lu$ . The magnetic structure is similar to that of  $CeCo_2Ge_4O_{12}$  rather than that of  $CeMn_2Ge_4O_{12}$ , which suggests that subtle structural variations are more important in determining the magnetic structure than is the electronic structure of the cations.

## References

- [1] T. Endo, Y. Doi, Y. Hinatsu, K. Ohoyama, *Inorganic Chemistry* 51 (2012) 3572-3578.
- [2] J.B. Forsyth, J.P. Wright, M.D. Marcos, J.P. Attfield, C. Wilkinson, *Journal of Physics-Condensed Matter* 11 (1999) 1473-1478.
- [3] G.J. Long, G. Longworth, P. Battle, A.K. Cheetham, R.V. Thundathil, D. Beveridge, *Inorganic Chemistry* 18 (1979) 624-632.

- [4] M.H. Whangbo, D. Dai, H.J. Koo, *Dalton Trans.* 2004 (2004) 3019-3025.
- [5] D. Xu, M. Avdeev, P.D. Battle, X.Q. Liu, *Inorg. Chem.* 56 (2017) 2750-2762.
- [6] D. Xu, M. Sale, M. Avdeev, C.D. Ling, P.D. Battle, *Dalton Trans.* 46 (2017) 6921 - 6933.
- [7] E.O. Wollan, W.C. Koehler, *Physical Review* 100 (1955) 545-563.
- [8] K. Momma, F. Izumi, *Journal of Applied Crystallography* 41 (2008) 653-658.
- [9] H.M. Rietveld, *Journal of Applied Crystallography* 2 (1969) 65 - 71.
- [10] A.C. Larson, R.B. von-Dreele *General Structure Analysis System (GSAS)* Los Alamos National Laboratories LAUR 86-748 1994
- [11] B. van Laar, W.B. Yelon, *J. Appl. Cryst.* 17 (1984) 47-54.
- [12] R.A. Brand <http://www.wissel-instruments.de/>
- [13] R.G. Burns, *Hyperfine Interactions* 91 (1994) 739-745.
- [14] D. DuBoulay, E.N. Maslen, V.A. Streltsov, N. Ishizawa, *Acta Crystallographica Section B-Structural Science* 51 (1995) 921-929.
- [15] M. Marezio, J.P. Remeika, P.D. Dernier, *Acta Crystallogr.* B26 (1970) 2008.
- [16] A. Masuno, A. Ishimoto, C. Moriyoshi, N. Hayashi, H. Kawaji, Y. Kuroiwa, H. Inoue, *Inorganic Chemistry* 52 (2013) 11889-11894.
- [17] V.G. Zubkov, N.V. Tarakina, I.I. Leonidov, A.P. Tyutyunnik, L.L. Surat, M.A. Melkozerova, E.V. Zabolotskaya, D.G. Kellerman, *Journal of Solid State Chemistry* 183 (2010) 1186-1193.

**Figure Captions**

- Figure 1 Crystal structure of  $AM_{2-x}M'_x\text{Ge}_4\text{O}_{12}$  viewed along (a) [100] and (b) [001].  $M/M'\text{O}_6$  octahedra,  $\text{GeO}_4$  tetrahedra and  $A$  atoms are coloured magenta, green and blue, respectively.
- Figure 2 (a) C-type antiferromagnetic structure of  $\text{CeMn}_2\text{Ge}_4\text{O}_{12}$ , (b) C-type structure of  $\text{CeMnCoGe}_4\text{O}_{12}$ , (c) mixed A- and G-type antiferromagnetic structure of  $\text{CeCo}_2\text{Ge}_4\text{O}_{12}$ . Only manganese and cobalt atoms are shown.
- Figure 3 Observed (red) and calculated (green) Cu  $K_\alpha$  X-ray diffraction profiles of  $\text{YMnFeGe}_4\text{O}_{12}$ . A difference curve is also shown. Vertical markers indicate reflection positions.
- Figure 4 Observed (red) and calculated (green) neutron diffraction profiles for  $\text{YMnFeGe}_4\text{O}_{12}$  recorded using  $\lambda = 1.622 \text{ \AA}$  at 300 K; a difference curve is also shown. Vertical markers indicate reflection positions.
- Figure 5  $^{57}\text{Fe}$  Mössbauer spectrum of  $\text{YMnFeGe}_4\text{O}_{12}$  collected at room temperature and fitted using a single quadrupole-split doublet component.
- Figure 6 Temperature dependence of the dc molar magnetic susceptibility of  $\text{LnFeMnGe}_4\text{O}_{12}$  for  $\text{Ln} =$  (a) Y, (b) Eu and (c) Lu.
- Figure 7 Field dependence of the magnetisation per formula unit of  $\text{LnFeMnGe}_4\text{O}_{12}$  for  $\text{Ln} =$  (a) Y, (b) Eu and (c) Lu.
- Figure 8 Frequency dependence of the ac molar magnetic susceptibility of  $\text{LuMnFeGe}_4\text{O}_{12}$ .
- Figure 9 Observed (red) and calculated (green) neutron diffraction profiles for  $\text{YMnFeGe}_4\text{O}_{12}$  recorded using  $\lambda =$  (a) 1.622 and (b) 2.4397  $\text{\AA}$  at 3.5 K; a difference curve is also shown. Upper and lower vertical markers indicate magnetic and structural reflection positions, respectively.
- Figure 10 The magnetic structure of  $\text{LnMnFeGe}_4\text{O}_{12}$  for  $\text{Ln} =$  Y, Eu and Lu; only Mn/Fe cations are shown.

**Table 1** Structural parameters derived from neutron diffraction data for  $LnMnFeGe_4O_{12}$  at room temperature

		<i>Ln</i>		
		Y	Eu	Lu
<i>Ln</i>	$U_{\text{iso}}/\text{\AA}^2$	0.0056(4)	0.0102(11)	0.0062(6)
Fe/Mn	$U_{\text{iso}}/\text{\AA}^2$	0.0052(8)	0.0078(20)	0.0065(11)
Ge	$x$	0.5227(1)	0.5259(2)	0.5210(1)
	$U_{\text{iso}}/\text{\AA}^2$	0.0042(2)	0.0049(5)	0.0042(2)
O1	$x$	-0.3688(1)	-0.3688(3)	-0.3694(1)
	$z$	0.1811(2)	0.1840(6)	0.1805(3)
	$U_{\text{iso}}/\text{\AA}^2$	0.0062(3)	0.0107(8)	0.0070(3)
O2	$x$	0.1611(1)	0.1606(3)	0.1614(1)
	$y$	0.0626(1)	0.0596(2)	0.0644(1)
	$z$	0.2574(2)	0.2561(6)	0.2592(2)
	$U_{\text{iso}}/\text{\AA}^2$	0.0096(2)	0.0119(4)	0.0098(2)
$a/\text{\AA}$		9.7259(1)	9.8083(3)	9.6662(1)
$c/\text{\AA}$		4.8130(1)	4.8030(2)	4.8158(1)
$V/\text{\AA}^3$		455.27(1)	462.07(3)	449.97(1)
$R_{\text{wpr}}$		3.84%	2.58%	4.58%
$\chi^2$		2.666	2.007	1.973

Space group  $P4/nbm$  (No. 125),  $Z = 2$ *Ln* on  $2b$  ( $\frac{1}{4}, \frac{1}{4}, \frac{1}{2}$ ); Fe/Mn on  $4f$  ( $0, 0, \frac{1}{2}$ ); Ge on  $8k$  ( $x, \frac{1}{4}, 0$ ); O1 on  $8m$  ( $x, -x, z$ ); O2 on  $16n$  ( $x, y, z$ )

**Table 2** Bond lengths (Å) and bond angles (degrees) in  $LnMnFeGe_4O_{12}$  at room temperature, derived from neutron diffraction data.

	$Ln$		
	Y	Eu	Lu
$Ln-O2 \times 8$	2.331(1)	2.372(3)	2.301(2)
Fe/Mn-O1 $\times 2$	2.369(1)	2.369(3)	2.357(1)
Fe/Mn-O2 $\times 4$	2.047(1)	2.049(3)	2.041(1)
Mean Mn/Fe - O	2.154	2.156	2.146
O2-O2' *	3.077(1)	3.055(4)	3.087(2)
O2-O2'' *	2.700(1)	2.730(4)	2.672(2)
Ge-O1 $\times 2$	1.792(1)	1.790(3)	1.792(1)
Ge-O2 $\times 2$	1.723(1)	1.728(3)	1.724(1)
O2-Fe/Mn-O2'	97.47(4)	96.43(10)	98.26(4)
O2-Fe/Mn-O2''	82.53(4)	83.57(10)	81.74(4)
O1-Fe/Mn-O2'	83.26(4)	84.05(10)	82.83(4)
O1-Fe/Mn-O2''	96.74(4)	95.95(10)	97.17(4)
O1-Ge-O1	107.81(5)	109.56(14)	107.51(6)
O1-Ge-O2	104.90(5)	105.00(14)	104.58(6)
O1-Ge-O2	108.04(5)	107.53(14)	108.33(6)
O2-Ge-O2	122.47(5)	121.91(14)	122.78(6)

\* distances within the equatorial plane of the (Fe/Mn)O<sub>6</sub> octahedra

**Table 3** Mössbauer parameters of  $\text{YMnFeGe}_4\text{O}_{12}$  at room temperature

$\delta / \text{mm s}^{-1}$	$ \Delta  / \text{mm s}^{-1}$	$\Gamma / \text{mm s}^{-1}$
0.407(2)	2.086(2)	0.376(4)

$\delta$  is the isomer shift, relative to  $\alpha\text{-Fe}$  at room temperature;  $|\Delta|$  is the magnitude of the electric quadrupole splitting and  $\Gamma$  is the full linewidth at half-maximum intensity.

**Table 4** Magnetic parameters of  $\text{LnMnFeGe}_4\text{O}_{12}$ 

	<i>Ln</i>		
	Y	Eu	Lu
$C / \text{cm}^3 \text{ K mol}^{-1}$	8.766(1)	8.758(1)	8.724(1)
$\theta / \text{K}$	-44.46(2)	-37.12(2)	-22.89(2)
$\mu^{(\text{Fe/Mn})}_{\text{eff}}$	5.92	5.92	5.91
$T_{\text{N}} / \text{K}$	16.0	17.0	15.0

**Table 5** Derived structural parameters for  $\text{ZrMn}_{2-x}\text{Co}_x\text{Ge}_4\text{O}_{12}$  [6],  $\text{CeMn}_{2-x}\text{Co}_x\text{Ge}_4\text{O}_{12}$  [5] and  $\text{LnMnFeGe}_4\text{O}_{12}$ 

Composition	$\langle r_{4f} \rangle / r_{2b}$	$2c/a$	$d(M_{4f}-\text{O}2)/d(M_{4f}-\text{O}1)$	$\varphi / ^\circ$	$\psi / ^\circ$	$q$
* $\text{ZrMn}_2\text{Ge}_4\text{O}_{12}$	0.988	1.0066	0.892(1)	78.18(12)	43.25(5)	0.870(1)
$\text{ZrMnCoGe}_4\text{O}_{12}$	0.938	1.0046	0.885(1)	78.68(12)	42.64(5)	0.859 (1)
$\text{ZrCo}_2\text{Ge}_4\text{O}_{12}$	0.887	1.0010	0.884(1)	79.42(12)	42.02(5)	0.850(1)
* $\text{CeMn}_2\text{Ge}_4\text{O}_{12}$	0.856	0.9974	0.879(1)	78.36(12)	42.04(5)	0.856(1)
$\text{CeMn}_{1.5}\text{Co}_{0.5}\text{Ge}_4\text{O}_{12}$	0.834	0.9950	0.876(1)	78.69(12)	41.60(6)	0.847(1)
$\text{CeMnCoGe}_4\text{O}_{12}$	0.812	0.9926	0.873(1)	78.32(22)	41.55(11)	0.838(2)
† $\text{CeMn}_{0.5}\text{Co}_{1.5}\text{Ge}_4\text{O}_{12}$	0.790	0.9902	0.874(1)	78.98(23)	41.04(12)	0.833(2)
† $\text{CeCo}_2\text{Ge}_4\text{O}_{12}$	0.768	0.9886	0.869(1)	79.18(13)	40.74(5)	0.831(1)
*† $\text{LuFeMnGe}_4\text{O}_{12}$	0.755	0.9954	0.866(1)	78.64(12)	40.78(5)	0.826(1)
*† $\text{YFeMnGe}_4\text{O}_{12}$	0.724	0.9888	0.862(1)	79.73(12)	40.28(5)	0.817(1)
*† $\text{EuFeMnGe}_4\text{O}_{12}$	0.692	0.9788	0.862(1)	81.11(28)	39.75(15)	0.803(2)

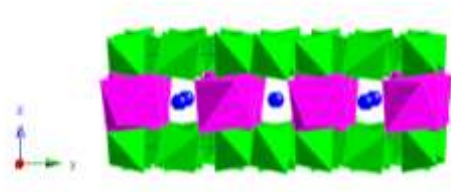
\*Compounds in which all the transition-metal cations have a  $d^5$  electron configuration

†Compounds where magnetic ordering is accompanied by a unit-cell doubling along [001].

 $\varphi$  Angle between  $M_{4f}-\text{O}1$  bond and  $M_{4f}-\text{O}2$  bond $\psi$  Angle between the  $M_{4f}-\text{O}1$  bond and the (001) plane $q$  Ratio of O2 – O2 distance in square face of antiprism to perpendicular distance between faces



(a)



(b)

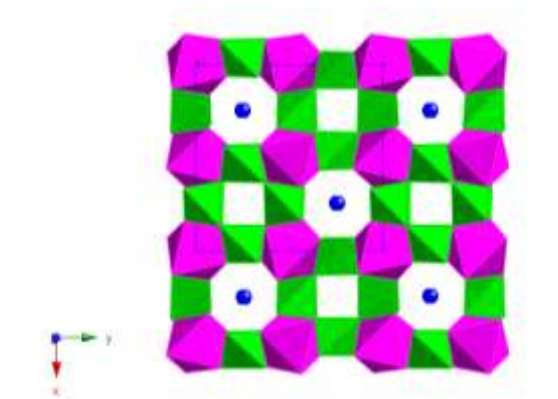
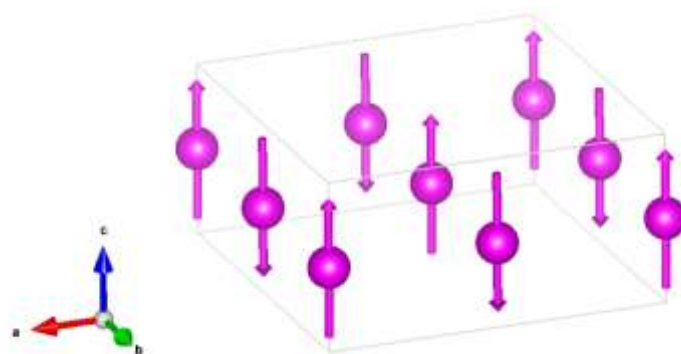
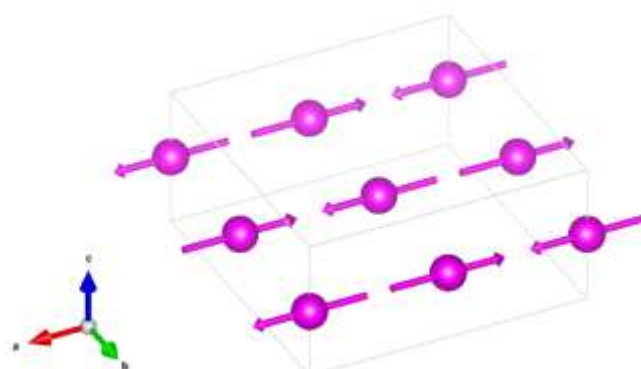


Figure 1

(a)



(b)



(c)

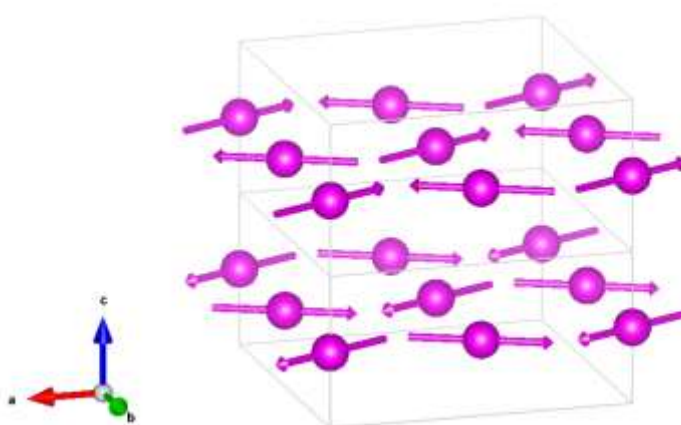


Figure 2

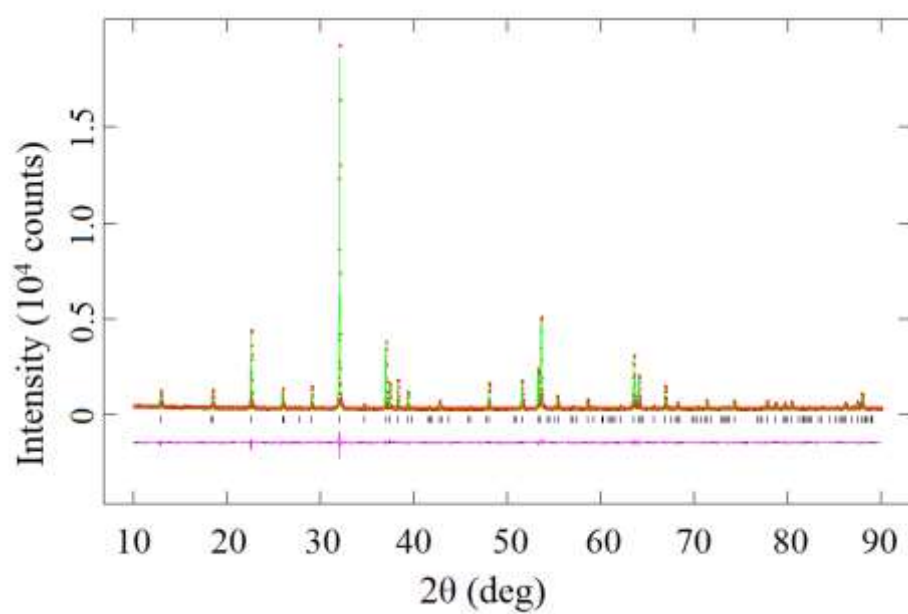


Figure 3

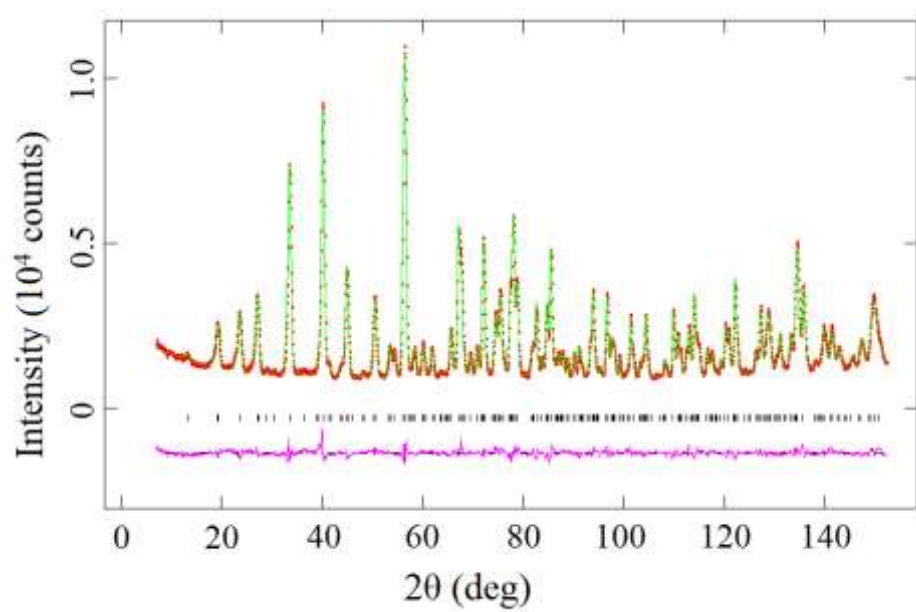


Figure 4

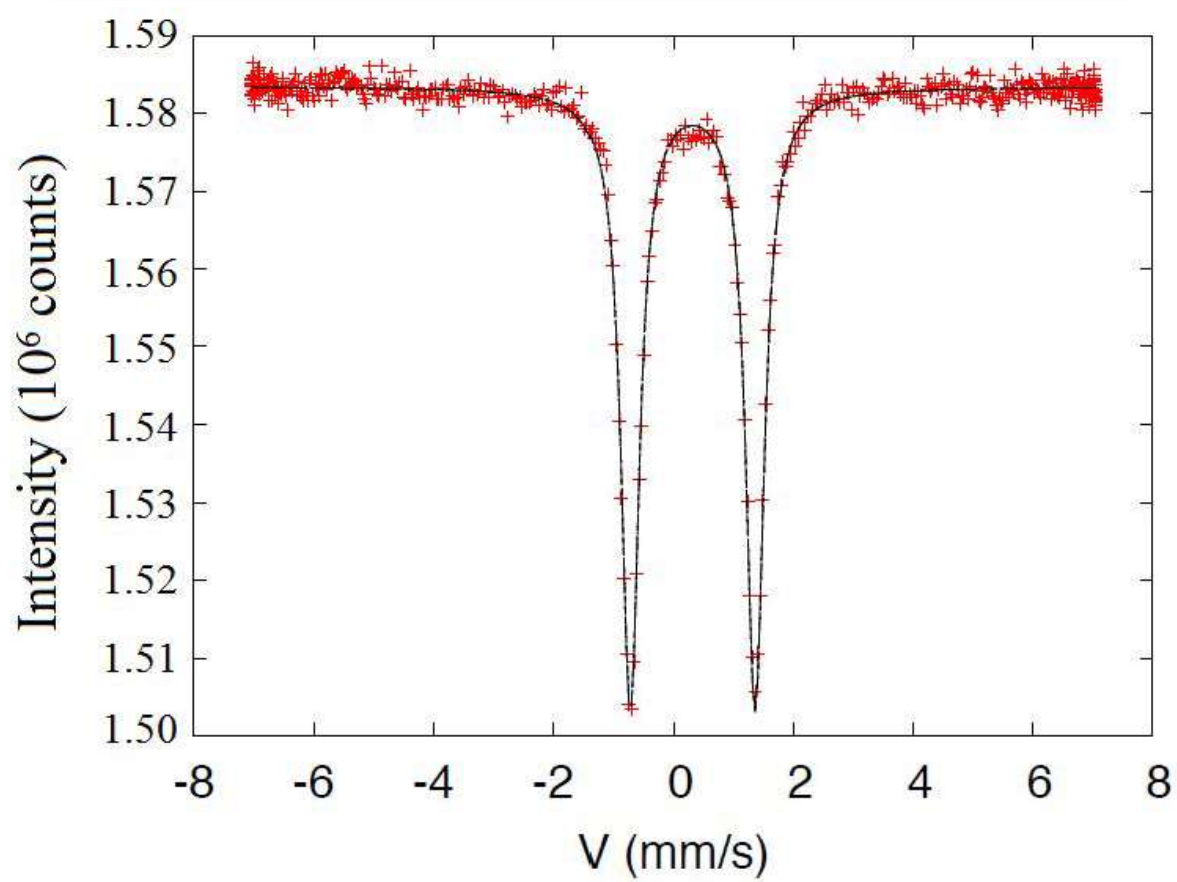
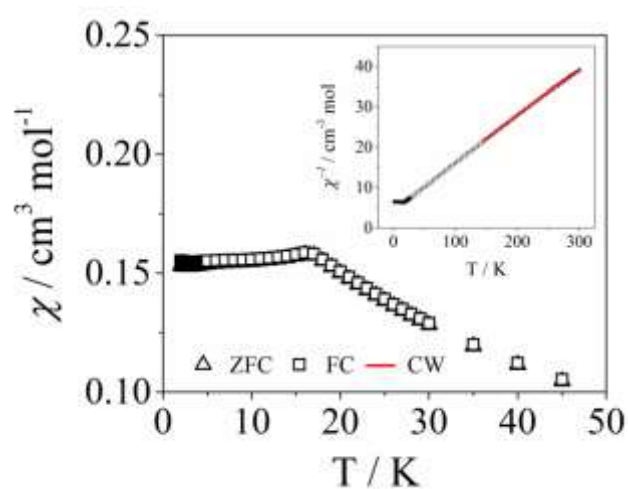
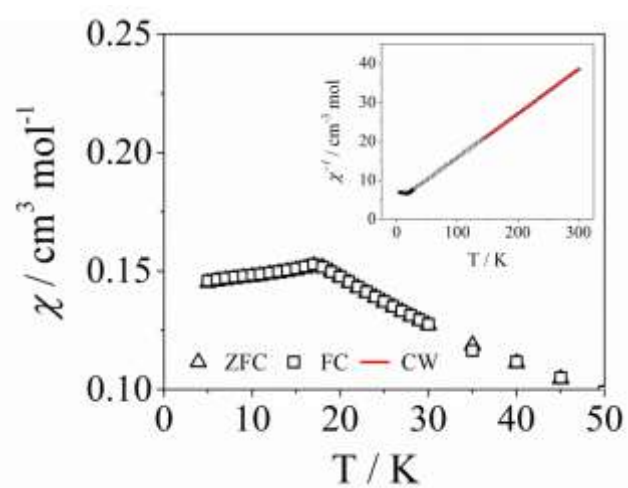


Figure 5

(a)



(b)



(c)

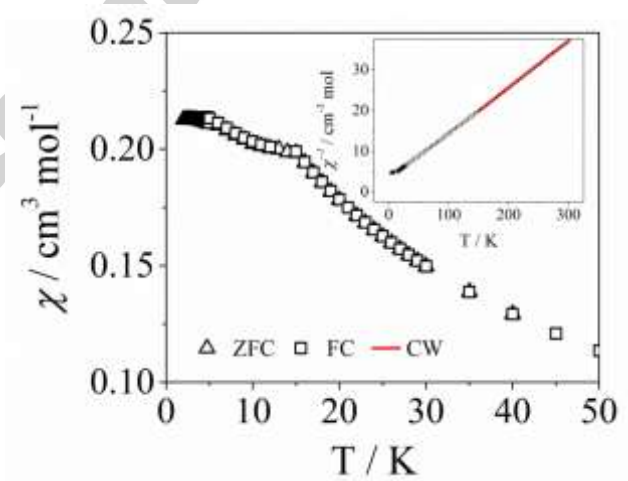
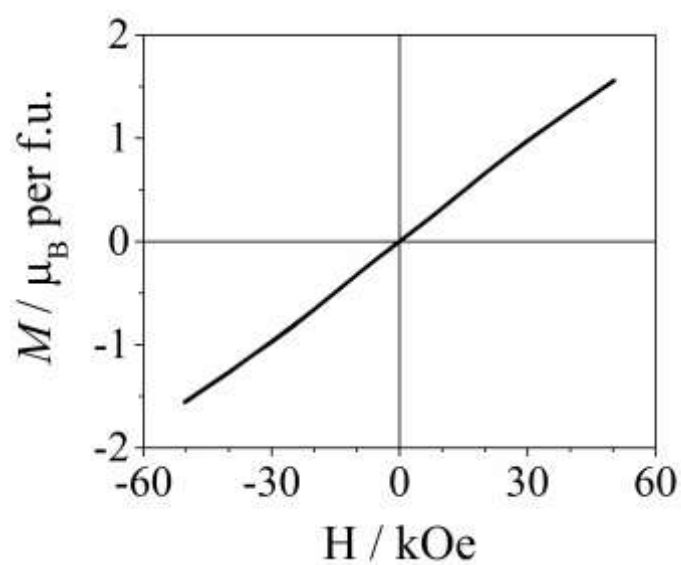
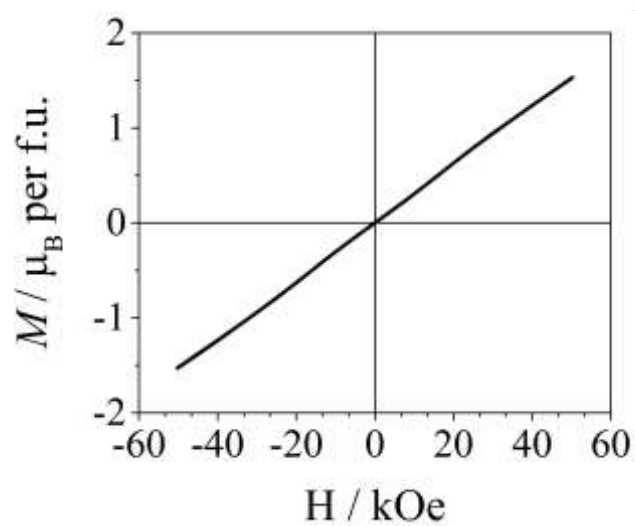


Figure 6

(a)



(b)



(c)

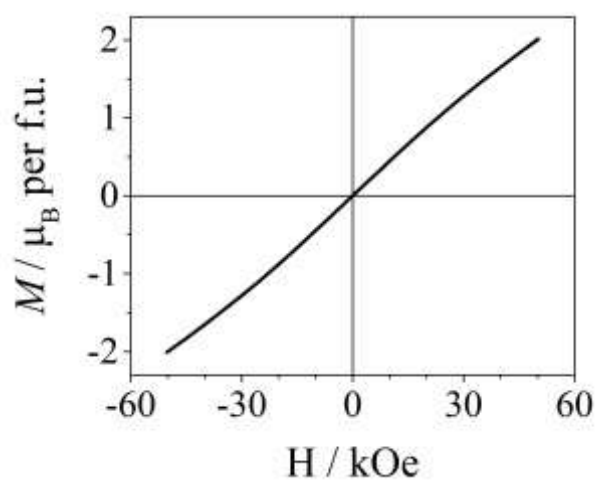


Figure 7

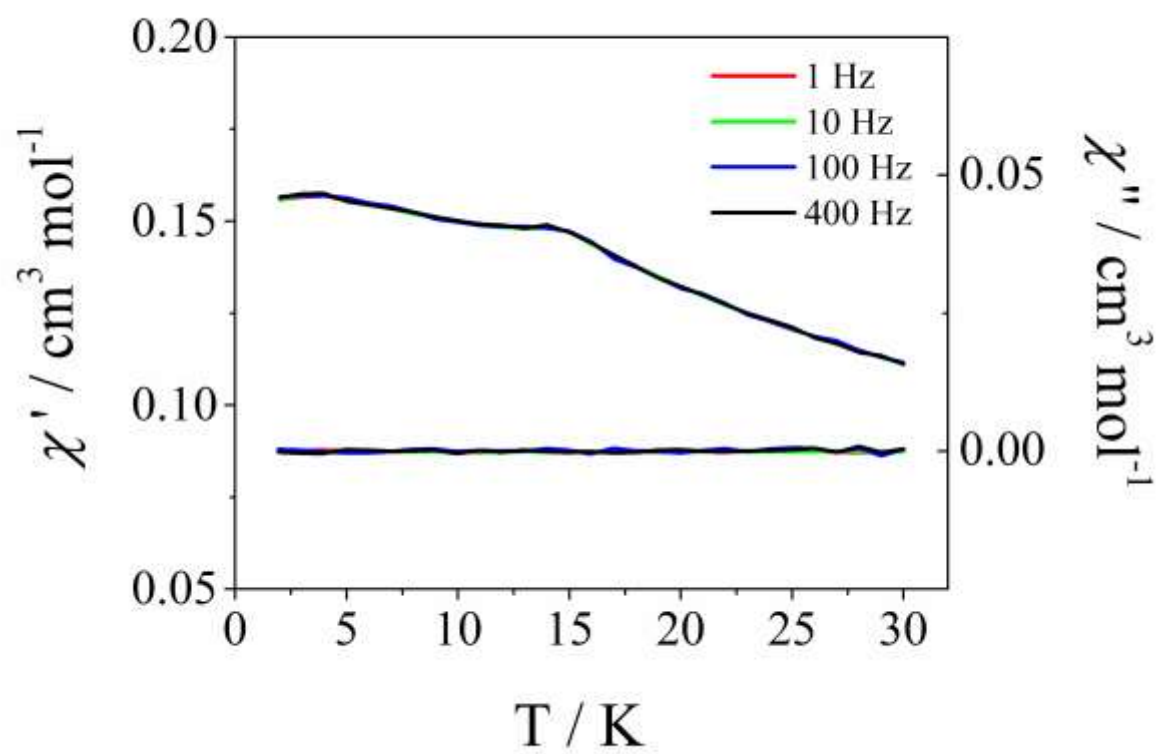
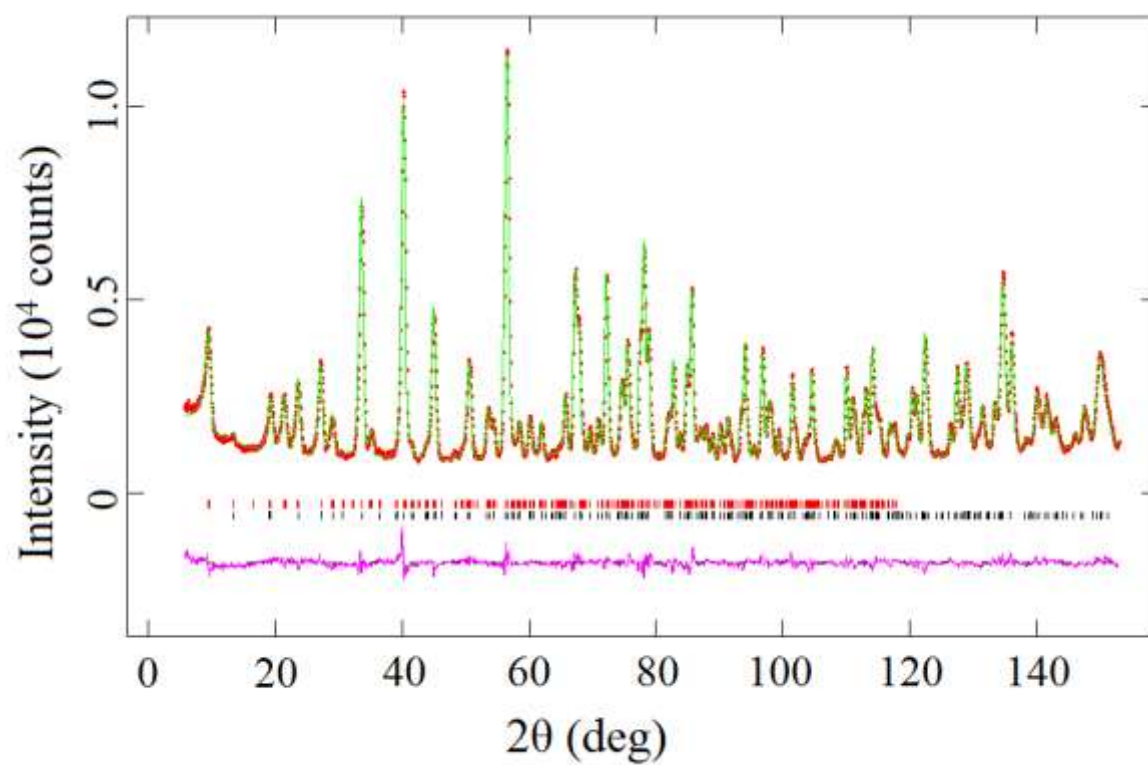


Figure 8

(a)



(b)

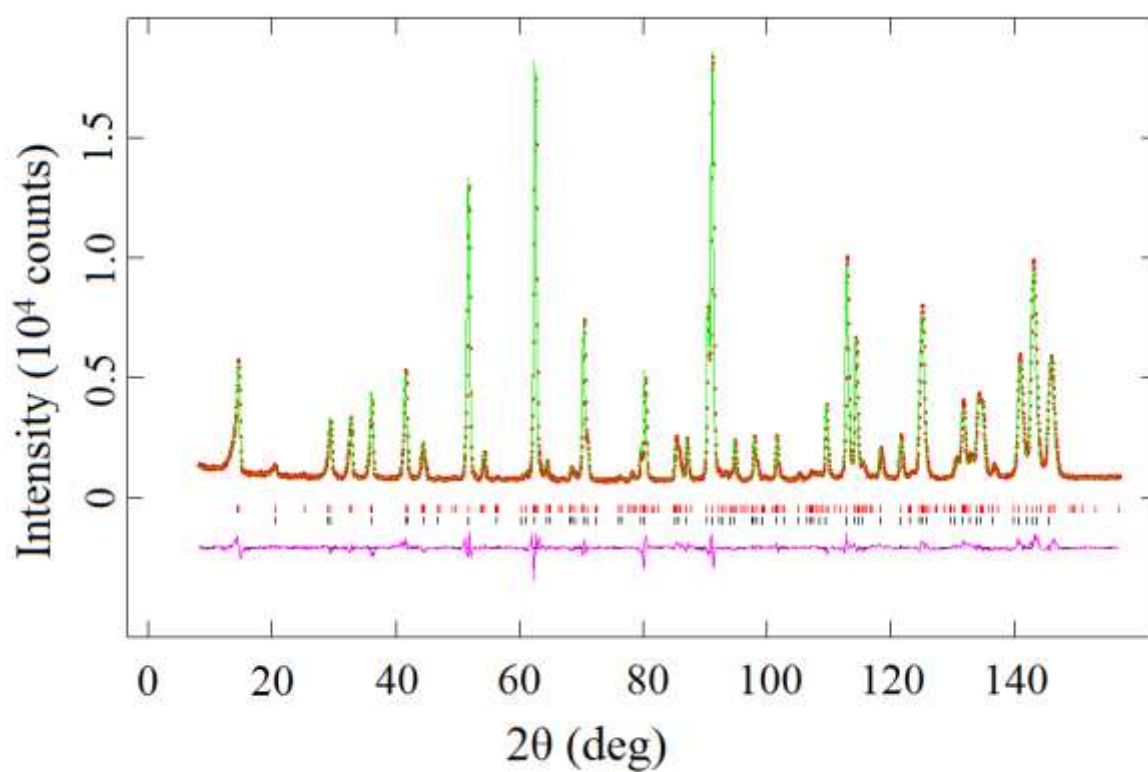


Figure 9



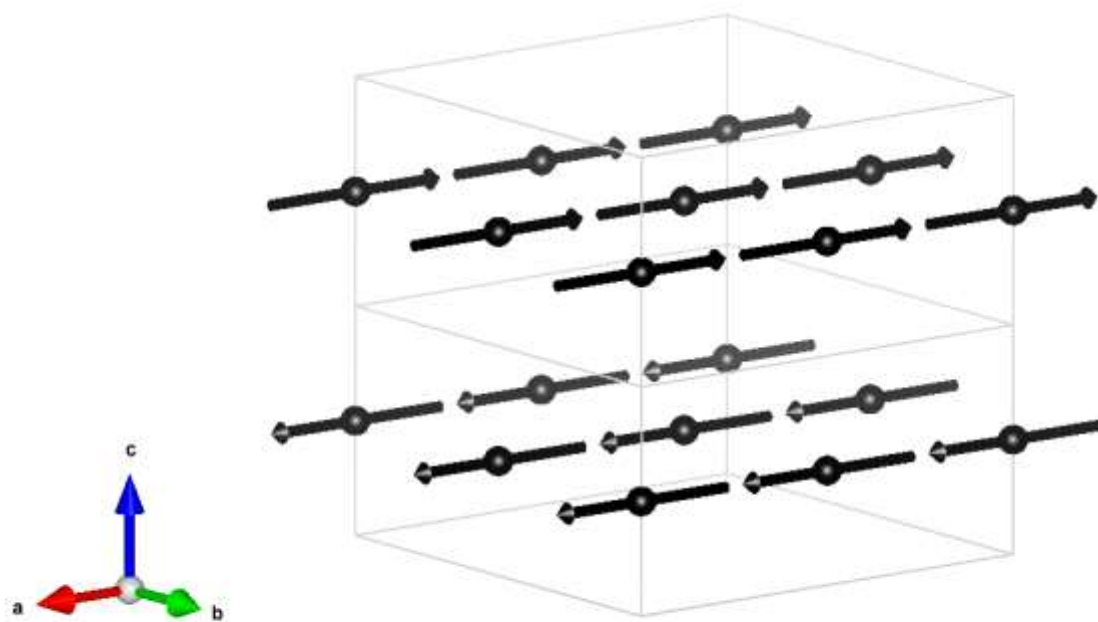


Figure 10

### Highlights

A-type antiferromagnetic ordering in mixed-metal germanates.

Unusually large isomer shift for  $\text{Fe}^{3+}$  in Mössbauer spectrum of  $\text{YMnFeGe}_4\text{O}_{12}$ .

Identification of factors that determine the magnetic structure adopted by compounds having this structure type.